Available online at www.sciencedirect.com
SCIENCE DIRECT®
Journal of Nuclear Materials 336 (2005) 97–109
journal of nuclear materials
www.elsevier.com/locate/jnucmat

Design feasibility study of a divertor component reinforced with fibrous metal matrix composite laminate

Jeong-Ha You *

Max-Planck-Institut für Plasmaphysik, EURATOM Association, Boltzmannstr. 2, D-85748 Garching, Germany

Received 18 May 2004; accepted 14 September 2004

Abstract

Fibrous metal matrix composites possess advanced mechanical properties compared to conventional alloys. It is expected that the application of these composites to a divertor component will enhance the structural reliability. A possible design concept would be a system consisting of tungsten armour, copper composite interlayer and copper heat sink where the composite interlayer is locally inserted into the highly stressed domain near the bond interface. For assessment of the design feasibility of the composite divertor concept, a non-linear multi-scale finite element analysis was performed. To this end, a micro-mechanics algorithm was implemented into a finite element code. A reactor-relevant heat flux load was assumed. Focus was placed on the evolution of stress state, plastic deformation and ductile damage on both macro- and microscopic scales. The structural response of the component and the micro-scale stress evolution of the composite laminate were investigated.

1. Introduction

1.1. Divertor components for power fusion reactors

In a future fusion reactor, which should furnish an electrical power of ≈1500 MW, the divertor will be exposed to quasi-stationary high heat flux (HHF) due to the bombardment by energetic particles. The deposited heat will be removed by active cooling to sustain the HHF loads.

A duplex bond joint structure has been a favourable design concept of the actively cooled divertor which consists of the plasma facing material (PFM) and the heat sink containing the cooling tube [1,2]. Such a bi-material structure was a necessary consequence to meet different physical and mechanical requirements [3–5]. Various types of the actively cooled duplex divertor have been developed primarily for ITER. These include flat tile type, mono-block type, lamellae mono-block type, macro-brush type, plasma sprayed coating type, etc. The thermal flow usually stagnates in the PFM, since the PFM typically has a smaller thermal conductivity than the heat sink material. As about 18% of the fusion power will be thermally exhausted through the divertor target plate, effective utilisation of the heat stored in the divertor coolant is an important concern for the operational efficiency of a power plant. The outlet coolant temperature should be high enough so that the extracted coolant heat can be directly used for the power generation. An estimate of the power plant efficiency was made in the frame of the European power plant conceptual study. In case of the model based on the

* Tel.: +49 89 3299 1373; fax: +49 89 3299 1212.
E-mail address: j.h.you@ipp.mpg.de

0022-3115/$ - see front matter © 2004 Elsevier B.V. All rights reserved.
doi:10.1016/j.jnucmat.2004.09.007

water-cooled lithium lead blanket (Model A), it was determined that the highest efficiency would be achieved at an outlet cooling water temperature of 325 °C in the divertor and the blanket [6]. However, this temperature was regarded as unrealistic, since the component temperature became too high for the considered heat sink material (copper alloy) to maintain its mechanical strength.

1.2. Loading environment and required material properties

The estimated data and the anticipated load parameters cited below refer to a typical power reactor. The maximum heat flux on the divertor target will reach up to 10–15 MW/m^2 under normal operation [7]. A steep temperature gradient and a mismatch in thermal expansion coefficients will cause significant thermal stresses including the residual stress. Such thermo-mechanical loads will be imposed in a quasi-cyclic mode (≈1000 cycles).

Due to the multiple loading conditions, the divertor structural materials should meet rather stringent qualification requirements. These are high temperature strength, low cycle fatigue (LCF) resistance, creep resistance and fracture toughness even under irradiation. The mechanical performance issue is mainly related to the structural part of the divertor. In the case of the flat tile type the PFM is used only as the functional part whereas the heat sink takes charge of the structural part. On the contrary, the PFM also plays the role of the structural part in the mono-block type.

Effective thermal performance is a critical concern for the divertor, since the thermal exhaust is the essential function of the divertor. Hence, superior thermal conductivity is of primary importance for the divertor heat sink material. The capability of rapid heat transport allows the coolant temperature to be increased so that the reactor efficiency can be enhanced.

Fast neutron environment raises one of the most crucial material problems, namely radiation damage. It is predicted that the annual neutron fluence will amount 5 MW/m^2 for the divertor. Intense fast neutron irradiation will cause extensive lattice displacement damage (50 dpa for the divertor after 5 years) and segregation of the transmutation helium gas (10 appm/dpa) [7]. These microstructural changes can result in serious deterioration of the important material properties, especially, decrease of the thermal conductivity, embrittlement (increase of the ductile-to-brittle transition temperature and loss of ductility) and swelling [7,8]. Such degradation features have a profound impact on the divertor performance in terms of the heat transport capability and the structural reliability. The component lifetime will be mainly limited by this factor. Reduced activation is an additional critical requirement. This safety criterion imposes a significant restriction on the availability of candidate materials. The allowable operation temperatures in the heat sink part rely on the embrittlement behaviour of the materials as well as the strength at this temperature range. Hence, one has to consider both the upper and lower limit of the temperature window.

The tungsten/copper system is one of the material options for the water-cooled ITER divertor (dome, baffles, the upper part of the vertical targets) [1]. It looks fairly probable that this material combination will be further considered for the design of the divertor of commercial reactors. In the following discussions, the related problems of the materials are addressed.

1.3. Tungsten for the plasma facing armour

Tungsten has been attracting increasing attention as a refractory PFM owing to its several conspicuous properties which are missing in other up-to-date PFMs [9,10]. High melting point, high thermal stress factor, low tritium inventory and low sputtering yield are the merits. Actually, tungsten is considered to be the most promising candidate for the PFM, although the experimental data from the fully tungsten-covered machines are incomplete yet [11]. Due to a very low erosion rate, the tungsten armour can be used in the form of a relatively thin layer (typically 3–5 mm scale). Tungsten does not undergo a sharp decrease of thermal conductivity under neutron irradiation. The activation property is relatively moderate.

On the other hand, there is a serious drawback in using tungsten as structural material of the divertor. Tungsten is brittle at low temperatures. Under intense neutron irradiation the DBTT (ductile-brittle transition temperature) is significantly increased [7]. It was observed that the radiation induced embrittlement occurred even up to 800 °C and already at low neutron dose (<1 dpa). This fact is actually the most vulnerable aspect for fusion application. Therefore tungsten might not be adequate for any structural application when the service temperature is low and large stresses with severe dpa damage are foreseen.

In the frame of the ITER divertor programme various types of the actively cooled tungsten divertor mock-ups were tested using HHF test facilities [12]. Both the mono-block type and macro-brush type showed no failure up to 1000 cycles under an absorbed heat flux of 14 MW/m^2. The plasma-sprayed type showed an inferior resistance compared to the former types. It sustained up to 5 MW/m^2 for 1000 cycles, which is below the divertor heat load regime. In general, the mono-block type showed better thermal fatigue resistance than the flat tile type. Extrapolation of these results to a reactor condition needs much caution, for the expected dpa damage and the resulting embrittlement are completely different. In the case of the tungsten mono-block type divertor com-

ponent, the tungsten temperature near the cooling tube remained cold during the heat flux loading. The temperature in this part was not much different from the coolant temperature. This temperature range is low enough to cause severe embrittlement. The thermal stresses are usually concentrated in the vicinity of the bond interface to the cooling tube due to the misfit in the CTEs. In the W/Cu mono-block divertor the residual stress will suppress the crack extension in tungsten during the cooling phase since the stress state is compressive. During the HHF loading, however, the temperature gradient can generate considerable secondary tensile stresses around the cooling tube. Under intense irradiation, the combination of cold embrittlement with tensile stress can be a critical situation.

On the other hand, tungsten shows rather high after heat emission. This suggests that a limited use of tungsten is desirable to avoid excessive after heat of the component. In these aspects, the flat tile type seems to be more preferable because here tungsten is used solely as PFM. There is a strong demand of new tungsten alloys which have sufficient ductility and toughness even after irradiation.

1.4. Copper alloys for the divertor heat sink

Materials selection for the divertor of commercial reactors is still an open question. Currently, there is no definite consent on it. This problem is attributed to the difficulty to find a material which fulfils all major requirements mentioned above. Copper alloys have been considered for the heat sink of the actively cooled flat tile type divertor in the long pulse fusion devices such as Tore Supra, W7X, JT60 and ITER [1,13–15]. In these machines the copper heat sinks have also structural function.

The excellent thermal conductivity of copper was the primary reason for the choice. In addition, copper shows a high swelling resistance under irradiation. On the other hand, the large thermal expansion coefficient (CTE) causes significant mismatch stresses upon temperature change when forming a bond joint with other materials having small CTEs. According to the experimental results from the numerous HHF cycling tests, the W/Cu divertor system withstood the device-relevant thermal loads with relatively low cooling water temperatures (below 100 °C) [12].

Two sorts of copper alloys have been considered: precipitation-hardened copper (CuCrZr alloy) and dispersion-strengthened copper (DS copper) [1]. There are two major drawbacks in using the copper alloys for reactor applications. The first is the relatively low and narrow operation temperature window and the second is the rather high long-term activation [10,16].

The former problem is directly connected to the radiation embrittlement and thermal softening. It was observed from neutron irradiation experiments (up to 10 dpa) that the irradiated CuCrZr alloy did undergo embrittlement below ≈250 °C and softening above 350 °C. Notable embrittlement begins already at low neutron fluence (0.3 dpa). Hence, to avoid an uncontrolled brittle fracture, the lowest temperature of the copper heat sink (which is almost equal to coolant temperature) should be higher than 250 °C. This temperature condition is also required for economic power plant operation. In this case, the irradiated copper heat sink becomes ductile so that the high temperature design rules can be applied. On the other hand, the upper service temperature limit will not be high enough, when the coolant temperature should exceed 250 °C.

So far, copper alloys have not been able to fully cover the high temperature strength requirements for reactor applications yet. It seems that the further gain in strength by means of the conventional metallurgical techniques is getting marginal. In this context, a new class of copper materials, for instance, fibre-reinforced composites, may come into question. It should be noted that thermal stresses generated by the CTE mismatch are concentrated locally in the vicinity of the bond interface. The dimensional extent of such a highly stressed region is usually small compared to the total volume of the bonded heat sink. This implies that only the region of stress concentration needs to be reinforced with high strength materials.

Regarding the activation problem, copper is not so favourable compared to the low activation materials such as reduced activation ferritic–martensitic steels (F82H, EUROFER), vanadium alloys or SiC/SiC composites. However, these three low activation materials possess poor thermal conductivity to be used for the divertor heat sink. In fact, no present candidate materials are able to satisfy all three essential requirements, namely, superior thermal conductivity, sufficient high temperature strength and reduced activation [17]. According to the DEMO divertor design study, the flat tile type W/F82H divertor could sustain only 3 MW/m^2 for a coolant temperature of 200 °C. In the case of the tungsten mono-block type with a steel cooling tube, the acceptable heat flux was raised up to 7–10 MW/m^2. These results show that the use of the ferritic–martensitic steels for the heat sink will require a more stringent restriction on the maximum allowable divertor heat flux compared to the copper heat sink.

The heat sink will be shielded from the plasma and be isolated from the other parts of the in-vessel components. Therefore radiological demerit of copper may be accepted as long as the total volume of the copper heat sink in the whole divertor cassette could be limited to a relatively small amount (say, 2–3 m^3) [2]. It is foreseen that the divertor component will be replaced periodically (e.g. 2–3 years cycle) [10].

1.5. New divertor concept based on a copper matrix composite

The foregoing discussions imply that the availability of reasonable structural materials is the key issue for the development of an innovative divertor. In general, fibre-reinforced metal matrix composites (FMMCs) show significantly improved strength and toughness in comparison to conventional alloys. Especially, the excellent creep resistance is the most noticeable feature [18]. Hence, an improvement of the structural performance of the divertor can be expected when reinforced with a FMMC.

In the last decade, intensive research work on the titanium-based FMMCs has been made in the aerospace sector. The technological feasibility of the titanium FMMC applied to the engine turbine rotor could be validated [19]. From this successful experience the development of a copper-based FMMC for the divertor application is motivated. Several important mechanical properties of a copper-based FMMC lamina estimated with the micro-mechanical theories are found in [20,21]. It was theoretically demonstrated that an enormous increase in the plastic work hardening rate and in the creep resistance could be achieved with a fibre volume fraction of 20%. The predicted plastic work hardening rate under axial tension reached 90 GPa, which was 30 times higher than that of copper alloy. The expected 50 000 h creep strain at 200 MPa and 400 °C was lower than 0.3%. The ultimate axial tensile strength (UTS) roughly followed the rule of mixture [18]. The initial yield stress strongly depends on the residual stress state [22]. This behaviour makes it difficult to predict a general trend of the global initial yield when only limited information is known about the residual stress. In [20], several estimated thermal and elastic properties of the copper FMMC lamina were reported. The axial elastic stiffness showed the rule of mixture dependence whereas the CTE showed a slight deviation from the linear dependence.

In this paper, we suggest a new divertor design which is based on the W/CuCrZr flat tile type. The essential feature is the local strengthening of the heat sink with a copper FMMC. The motivation of this concept is to endow the heat sink with sufficient high-temperature strength without notable decrease of thermal conductivity. The aim of this study is to evaluate the design feasibility of the FMMC-reinforced divertor concept in terms of composite reliability and structural integrity. In addition, the effect of the FMMC interlayer on the temperature and the stress within the component was assessed assuming a reactor-relevant HHF load. To this end, the non-linear multi-scale finite element analysis (NLMS-FEA) was performed to trace the damage evolution on a microscopic scale. Also a fracture mechanical study was carried out. Comparative assessment was made between the FMMC-reinforced divertor model and a conventional model having the same geometry but without FMMC. For compactness, the details of the theoretical background will not be presented.

2. Geometry, materials and loads

The reference geometry of the present model was based on the ITER divertor [2]. The geometry of the FMMC-reinforced model is shown in Fig. 1. This model was an actively cooled tri-material system which consisted of tungsten PFM armour, FMMC interlayer and copper heat sink. For comparative studies, a separate model having the identical geometry but without the FMMC interlayer was investigated in parallel. The considered armour thickness (10 mm) was larger than necessary for the erosion lifetime (<5 mm). The thicker tungsten PFM will generate accordingly higher thermal stresses in the FMMC interlayer. Hence, a conservative damage estimation will be made in this case.

Stress-relieved pure tungsten was chosen for the PFM and precipitation hardened CuCrZr alloy for the heat sink. A 3 mm thick planar layer of the fibre-reinforced copper matrix composite laminate was inserted between the PFM and the heat sink. This FMMC layer was assumed to be a cross-ply stacking (that is, [0°/90°] sequence) of the unidirectional composite laminae consisting of CuCrZr alloy matrix and continuous SiC fibres

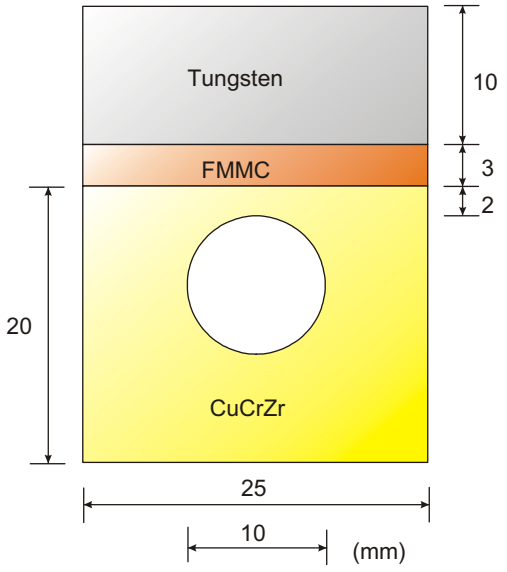

Fig. 1. Geometry of an actively cooled divertor model considered for present analysis. This divertor system consists of tungsten armour, copper-based composite laminate layer and copper alloy heat sink.

Table 1
Selected material properties[a] [18,35]

	Tungsten[b]	CuCrZr	SiC fibre
Young's modulus (GPa)	398	128	430
Yield stress (MPa)	1350 (20 °C)	300 (20 °C)	
	1100 (250 °C)	250 (250 °C)	
	680 (700 °C)	100 (700 °C)	
Work hardening rate (MPa) (up to 10% plastic strain)	2600 (320 °C)	1050 (20 °C)	
	1800 (530 °C)		
Thermal conductivity (W/m K)	170 (20 °C)	380 (20 °C)	16
	100 (2000 °C)	350 (400 °C)	
CTE[c] (10^{-6}/K)	4.5	15.7	5.7

[a] Room temperature values, if not indicated.
[b] Stress-relieved pure tungsten.
[c] Coefficient of linear thermal expansion.

with a volume fraction of 20%. The CuCrZr alloy was chosen for the matrix because it possesses nearly eight times higher yield stress than that of annealed pure copper. Selected material properties are summarised in Table 1. For simplicity, perfect bonding of the fibre/matrix interface was assumed. This rather crude simplification might be justified by the loading nature of the cross ply FMMC laminate. The applied forces will be born primarily in the axial directions of the fibres. Furthermore, there exists a rather strong compressive radial residual stress acting perpendicular to the fibre/matrix interface. In combination with a high interfacial bond strength this compressive radial stress component suppresses the debonding or sliding at the interface.

The loading condition considered for the thermal stress analysis is listed in Table 2. A uniform heat flux load of 15 MW/m^2 and a cooling water temperature of 250 °C (pressure: 4 MPa) were assumed. This heat flux is the upper limit expected for reactor normal operation. For the prescribed heat flux the assumed coolant temperature 250 °C was nearly the maximum value to be applied. When the coolant temperature was higher than 250 °C, the temperature of the FMMC layer would exceed the fabrication temperature (≈700 °C).

For the given maximum allowable FMMC temperature the present loading condition will produce the strongest temperature gradient and hence the largest secondary (thermal) stresses. Therefore, the damage assessment from this loading condition will lead to a conservative evaluation of the design feasibility.

The coupled thermal stress analysis consisted of two steps: preceding thermal analysis and subsequent stress analysis. Residual stresses to be generated by the joining process (i.e. uniform cooling from the fabrication temperature) were also considered. The stress-free temperature was assumed to be 700 °C. The secondary stresses caused by the HHF load were superposed onto the previous residual stresses.

Table 2
Load condition used for the high heat flux loading simulation

Heat flux (MW/m^2)	15
Pulse duration (s)	30
Coolant temperature (°C)	250
Stress free temperature (°C)	700

3. Computation

In the framework of NLMS-FEA (non-linear multi-scale finite element analysis), the field quantities (stress, strain) are simultaneously computed on the micro- as well as on the macro-scales. Emphasis was placed on the local evolution of the stress state, the plastic deformation and the ductile damage under the prescribed thermal load. The computational procedure of the NLMS-FEA consisted of two steps: (1) finite element analysis of the global stress states and (2) micro-mechanical computation of the local stress states in the individual phases (matrix and fibres). The temperature dependence of the material parameters was taken into account.

Since the matrix behaviour was assumed to be elastic–plastic, a rate form of the micro-mechanical constitutive equation had to be applied. In the practice, the rate form was replaced by an incremental form. The Mori–Tanaka mean field theory was used for the micro-mechanical computation step [23]. The incremental computation of the Mori–Tanaka mean field formulations required numerical integration of the Eshelby tensor [24]. The incremental Mori–Tanaka mean field algorithm was implemented into the commercial finite element code ABAQUS as a user-defined material subroutine [25]. This algorithm was originally developed by Pettermann et al. [26]. A schematic flow chart of the computational procedure is illustrated in Fig. 2. The Prandtl–Reuss flow theory was used for the matrix

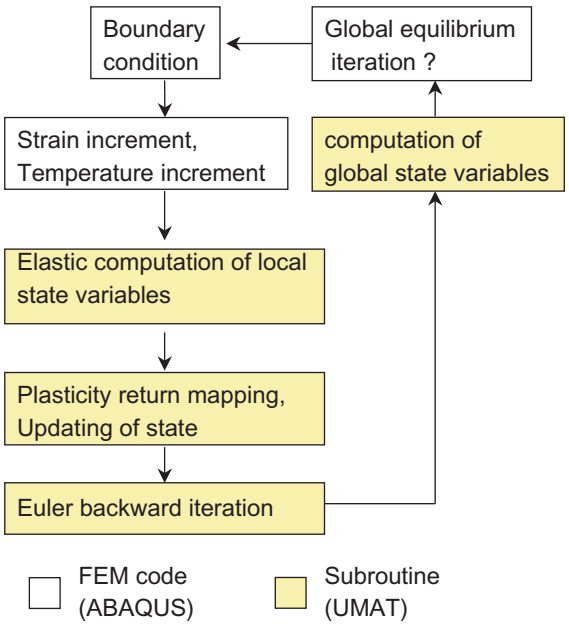

Fig. 2. Structure of the computational procedure for elastic–plastic multi-scale finite element analysis. UMAT is a user-defined subroutine of ABAQUS code for material constitutive equation. The steps which are performed with UMAT are indicated with shaded boxes while the steps of standard finite element computation are shown with white boxes.

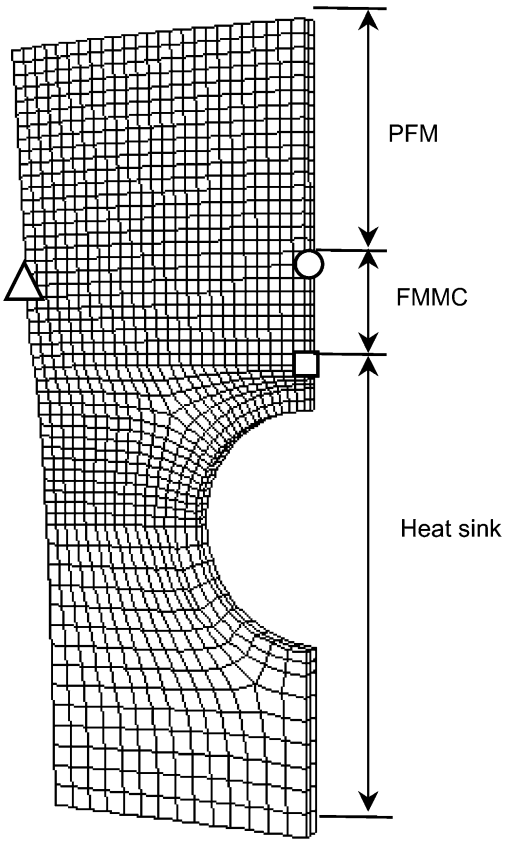

Fig. 3. Finite element mesh for the three-dimensional divertor model used for the dual scale thermal stress analysis.

plasticity. Additional internal iterations had to be performed for each increment to correct the characteristic Euler-backward behaviour of the global composite stress caused by the matrix stress updating after plastic yield.

The finite element mesh in a typically deformed structure under the assumed HHF load is shown in Fig. 3. Due to the two-fold symmetry only half of the component was modelled. Kinematic constraints were applied to keep the cross-sections planar. The number of elements and nodes amounted to 2300 and 17 700, respectively. Coupled with the user-defined material subroutine, three-dimensional composite laminate elements were used for the FMMC, while second-order hexahedral continuum elements were used for other parts [25]. The total computation time of a single job takes 227 h on a SUN Ultra60 workstation.

For the verification of this new numerical technique in which the NLMS-FEA algorithm was combined with the composite laminate elements, a series of test simulations were carried out for typical titanium matrix FMMC laminates for which reliable experimental data could be found in literature. Various thermal or thermo-mechanical load cycles were simulated. It turned out that the present technique could reproduce the stress–strain responses in good agreement with the experimental results. One representative result is shown in Fig. 4. The considered FMMC was a cross ply laminate system consisting of Timetal21S (metastable β-titanium alloy with the chemical composition of Ti15-Mo2.7Nb3Al0.2Si) matrix and SiC fibres (high modulus SCS6 grade with fibre diameter of 140 μm) with a fibre volume fraction of 35%. The assumed stress free temperature was 815 °C, which was identical to the specific processing temperature for the titanium FMMC as reported in the literature. It was assumed that the composite laminate was subjected to a uniaxial in-plane tensile loading–unloading cycle at 650 °C. It is shown that a good agreement was obtained between the simulation and the experiment [27]. However, this method could not be validated for cyclic loading cases.

For a fracture mechanical investigation, an interfacial crack with length of 0.5 mm was introduced at the free edge of the bond interface. Contact elements were used for the crack faces. The J integral and the complex stress intensity factor were determined assuming linear elastic material behaviour and using the homogenised FMMC properties. In addition, the stress singularity near the free surface edge of the perfectly bonded inter-

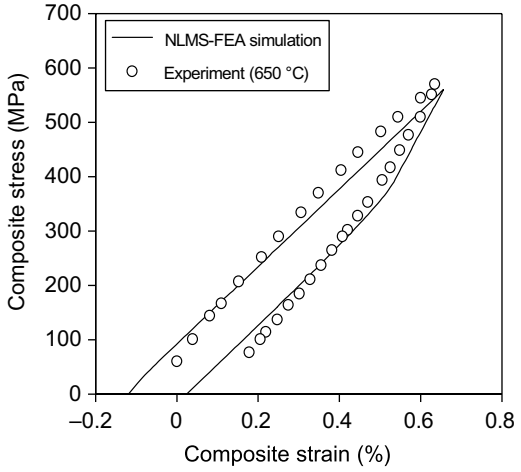

Fig. 4. Comparison between the computed and measured stress–strain curve of a fibrous titanium matrix composite with a fibre volume fraction of 35%. Uniaxial tensile loading–unloading test at 650 °C was simulated. Cross-ply laminate structure with stress-free temperature of 815 °C was assumed according to literature data.

face was also analysed. The fracture mechanical parameters characterising the singular stress fields were determined.

4. Results and discussion

4.1. Preliminary investigations on the W/CuCrZr system

From the finite element analysis it was observed that the stress history path at the heat sink interface of the W/CuCrZr system is well beyond the allowed stress limit (e.g. ITER design criterion S_m) under the given heat load condition. In fact, considerable plastic flow took place in the heat sink of the W/CuCrZr system. The plastic strain was mainly concentrated in the vicinity of the bond interface, especially near the free surface edge of the interface leading to a flow localisation. In this region, the accumulated equivalent plastic strain amounted to 5–20% at the end of the load cycle. Though the dimension of the singular fields was relatively small compared to the whole interface dimension (≈5%), it was large enough to have structural importance. The other part of the heat sink experienced far less plastic flow. For example, the equivalent plastic strain in the interfacial region outside the singular fields amounted to 2–5%. It is expected that the accumulated plastic strains will increase from cycle to cycle. The large amount of the plastic strain in the highly stressed heat sink interfacial region of the W/CuCrZr system strongly suggests the necessity of local strengthening.

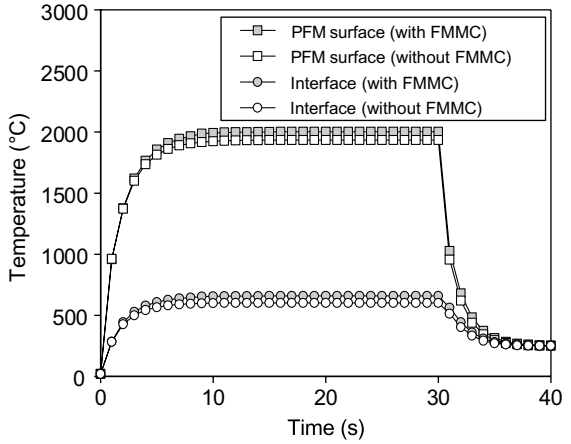

Fig. 5. Temperature development of the two considered divertor models simulated for the heat flux load of 15 MW/m^2 with coolant temperature of 250 °C. Temperatures are plotted at the armour surface and at the bond interface.

4.2. Effect of the FMMC layer on the component temperature

The computed temperature cycles at the PFM surface and at the bond interface of the PFM are plotted in Fig. 5. The result for the W/FMMC/CuCrZr system is compared to those for the W/CuCrZr system. The temperature difference between both systems was less than 70 °C at both locations. This fact indicates that the influence of the FMMC layer on the heat removal capability of the component was relatively small.

It is the temperature at the PFM/FMMC interface that has a structural importance since the difference between the fixed stress free temperature and the instantaneous temperature determines the overall thermal stress due to the mismatch in the CTE. This so-called mismatch thermal stress usually concentrates near the bond interface. The temperature at the PFM/FMMC interface attained 660 °C which was very close to the assumed stress free temperature. In this case, the mismatch stress almost disappeared according to the decreasing temperature difference while the secondary stress induced by the temperature gradient becomes dominant as will be shown later.

The maximum heat sink temperature in the W/FMMC/CuCrZr system reached 500 °C at the FMMC/heat sink interface.

4.3. Effect of the FMMC layer on the heat sink stress

The peak heat sink temperature seems to be too high for the copper alloy to be used as structural body. In the current case of the W/FMMC/CuCrZr system, however, the stresses in the whole heat sink actually vanished

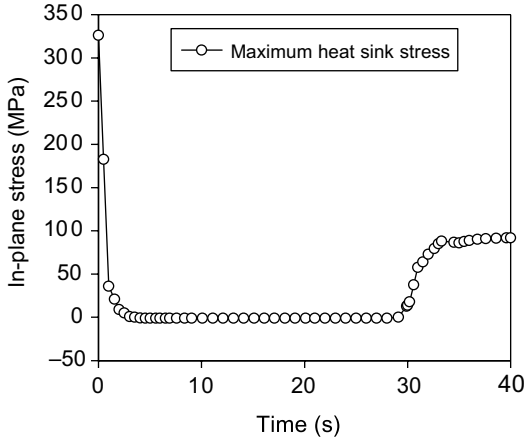

Fig. 6. Evolution of the typical thermal stress (in-plane normal component) in the copper heat sink of the W/FMMC/CuCrZr system at the position indicated by a square in Fig. 3 (heat load: 15 MW/m^2).

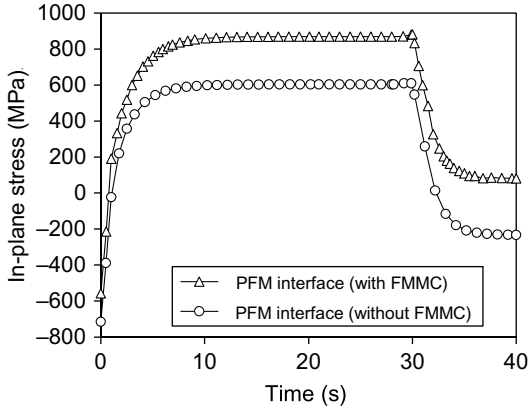

Fig. 7. Stress evolution in the tungsten PFM at the bond interface position indicated by a circle in Fig. 3. Results are compared for both the W/CuCrZr system and the W/FMMC/CuCrZr system.

during the HHF loading (see Fig. 6). The stresses in the heat sink were not really notable until the component was cooled down. This situation is analogous to a pure heating of the alloy. This fact implies that the moderate temperature increase caused by the FMMC layer will not significantly affect the strength of the heat sink. The statement is also valid for the expected heat flux range (10–15 MW/m^2) since the stress in the heat sink remains still small during heat loading. The heat sink stress was even slightly relieved by the FMMC layer.

4.4. Effect of the FMMC layer on the PFM stress

Because the most stressed region is located in the vicinity of the bond interface, the stresses at this position is most informative for the assessment of the structural effect of the FMMC layer.

The evolution of the thermal stresses in the tungsten PFM at the bond interface (circle position in Fig. 3) is shown in Fig. 7. In-plane normal component parallel to the interface is plotted for both the W/CuCrZr system and the W/FMMC/CuCrZr system. The initial stresses at the beginning of the load cycle denote the residual stresses at room temperature.

The comparison revealed the apparent effect of the FMMC layer on the PFM stress. The most salient feature was the remarkable increase of the tungsten interfacial stress due to the FMMC layer as a result of the HHF loading. This does not well accord with our physical intuition remembering that the FMMC layer would weaken the mismatch of the CTE (and also the elastic constants) between the PFM and the heat sink. Actually, the residual stresses in tungsten where the temperature field was uniform was indeed diminished by the FMMC layer. This means that the W/FMMC/CuCrZr system would generate smaller thermal stress than the W/CuCrZr system, if the changing temperature field remained uniform. In contrast to the uniform heating (or cooling) case, the HHF load produced an extremely steep temperature gradient which induces a forced bending moment [28]. The secondary stress caused by this bending moment is proportional to the stiffness of the partner material. For the case of a bi-material joint system, the thermal stress at the interface caused by a given bi-linear temperature gradient can be expressed by [29],

$$\sigma^i_{\mathrm{PFA}} = E'_{\mathrm{PFA}}\left[\frac{\alpha_{\mathrm{HS}}\Delta T_{\mathrm{HS}} - \alpha_{\mathrm{PFA}}\Delta T_{\mathrm{PFA}}}{1 + \dfrac{E'_{\mathrm{PFA}}}{E'_{\mathrm{HS}}}\dfrac{h_{\mathrm{PFA}}}{h_{\mathrm{HS}}}} + \alpha_{\mathrm{PFA}}(\overline{T}_{\mathrm{PFA}} - T_{\mathrm{i}})\right]. \tag{1}$$

The notations used in the equation are as follows. σ^i_{PFA}: the PFM stress at the bond interface, E': the effective elastic modulus, α: the CTE, h: the thickness, ΔT: the difference between the mean temperature of a layer and the reference (or the stress free) temperature, $\overline{T}$: the mean temperature of a layer and T_{i}: the temperature at the bond interface.

This equation shows the proportional relationship between σ^i_{PFA} and E'_{HS}. The elastic stiffness of the FMMC amounts to 176 GPa, which is by 38% higher than the elastic modulus of the copper alloy. The relative increase in the tungsten interface stress due to the FMMC layer was 44%. This result supports previous interpretation.

While the in-plane normal stress at the tungsten bond interface amounted to 870 MPa, the equivalent stress at this position reached 650 MPa which was within the elastic limit at the peak temperature. For irradiated tung-

sten, brittle failure criteria would be more appropriate. The influence of the FMMC layer on the tungsten PFM stress should be assessed carefully since the stress at the PFM interface was tensile during the HHF loading. In the practical application, the thickness of the PFM and of the FMMC interlayer should be optimised so that the tungsten interface stress does not exceed the failure criterion.

Here, the stress of the tungsten PFM was discussed only in the comparative sense to evaluate the structural effect of the FMMC layer without making any failure prediction.

4.5. Evolution of FMMC stresses on meso- and micro-scales

In the W/FMMC/CuCrZr system, the FMMC was assumed to consist of cross-stacked laminae. Each finite element for the FMMC corresponds to a composite laminate consisting of six cross-ply laminae. In this case, the real stress profiles will show very complicated patterns which are essentially affected by the spatial arrangement of the laminae. The fluctuating stress distribution will reveal three different hierarchial length scales: the finite element edge length scale (macro), the lamina thickness scale (meso) and the fibre radius scale (micro). The NLMS-FEA covers all these three length scales. For a comprehensive interpretation the stresses of specific geometrical entities having different dimensional scales are expressed using a volume average homogenisation scheme based on that specific length scale under consideration.

Now, the stress behaviour of the FMMC itself is examined. To depict the stress fluctuations with spatial resolution of lamina thickness length scale, the stresses were homogenised for each lamina in the laminate.

The evolution of the lamina stresses in the laminate element near the bond interface (circle position in Fig. 3) is shown in Fig. 8. The plotted stresses are the lamina in-plane component for two different stacking positions located at the bottom and at the middle of the laminate element. For comparison, the heat sink stress of the W/CuCrZr system at the same interface position is also plotted.

Significant difference is seen in the lamina stresses for the whole load cycle although the distance between the considered lamina positions was very short (<0.3 mm). Such a rather anomalous short range stress fluctuation is the characteristic feature of a FMMC laminate which can be readily explained based on the classical laminate theory. At the current stage of meso-scale stress analysis, a simple failure prediction can be made by comparing the computed lamina stress with measured lamina strength data. In general, the strength data of a lamina can be obtained in more straightforward manner than

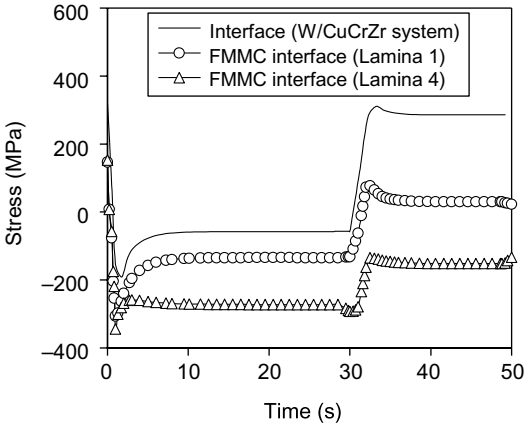

Fig. 8. Stress evolution in the composite laminate near the bond interface (circle position in Fig. 3). The stresses are expressed as homogenised lamina in-plane stress for two different lamina stacking positions. The heat sink stress of the W/CuCrZr system at the same position is also plotted for comparison.

a laminate. But, plastic damage of the matrix cannot be sensibly captured in the ultimate strength data.

Another important point during the heat flux loading is that the FMMC near the interface was more intensively stressed in compression than the heat sink of the W/CuCrZr system at the same position. This effect has the same physical origin as the increase of the PFM interface stress. On the contrary to the tungsten interface stress, the increase of the lamina stress is not particularly critical because the laminae were loaded mostly

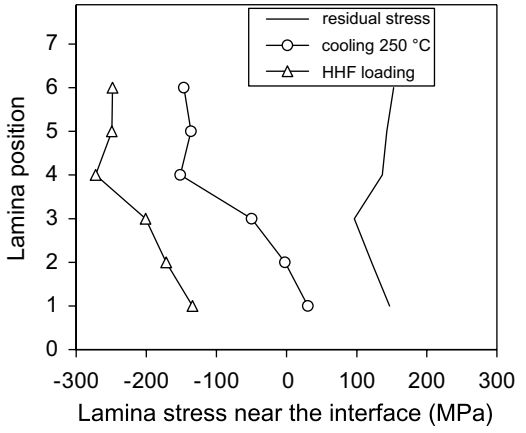

Fig. 9. Stress profiles in the composite laminate near the bond interface (circle position in Fig. 3). The profiles correspond to the stacking direction. The stresses are expressed as homogenised lamina in-plane stress. The stresses are compared for three different stages namely, the residual stress state, heat flux loading state and cooling state.

in compression, as will be shown in Fig. 9. In the cooling phase, the W/FMMC/CuCrZr system produced much more favourable stress states in the laminae than in the heat sink of the W/CuCrZr system as the stress state was shifted to a compressive regime in the laminate element. The vertical stress profiles in the laminate element at the circle position of Fig. 3 are plotted in Fig. 9. Each data point denotes the lamina in-plane stress at the corresponding stacking position. The individual stress profiles stand for the three representative stages of the load cycle namely, the residual stress state (at RT), the heat flux loading state and the cooling state. By comparing the three profiles the change of the internal stress distribution in the laminate element during the thermal load cycle can be recognised. As already shown in the previous figure, the profiles reveal remarkable stress gradients. Near the bond interface, the laminae were mostly stressed in compression during the heating phase.

Up to now, the lamina stresses in the FMMC were examined based on the meso-scale homogenisation. Next, the stresses in the FMMC on the micro-scale are investigated in order to identify separately the stress of the fibres and of the matrix. Such a microscopic resolution of the laminate stress allows a failure prediction for which only the failure properties of the individual constituent materials are needed. This is a remarkable advantage because the data on fracture or damage for the fibre or for the matrix can be more readily obtained than for their composites.

The evolution of the microscopic stresses in the matrix and the fibres is plotted for the near-interface position in Fig. 10, (the circle position in Fig. 3). During the whole heat load cycle the fibre axial stress remained in compressive state while the sign of the matrix stress was reversed from tension to compression upon heating. Analogous to the lamina stress case, the reversion of the stress sign in the matrix was attributed to the forced bending of the joint caused by the temperature gradient.

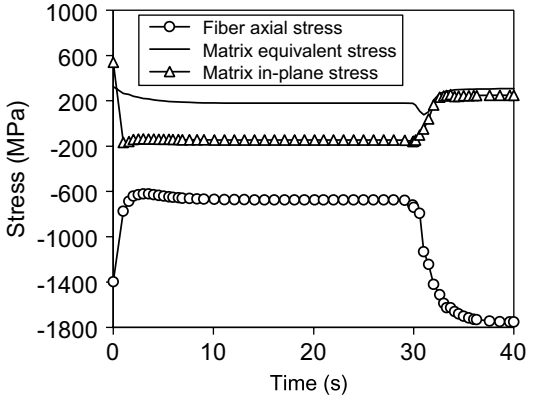

Fig. 10. Stress evolution in the fibre and in the matrix of the composite laminate at the interfacial position indicated by a circle in Fig. 3.

The fibre stress was significantly diminished upon heating. The maximum fibre stress amounted to 1800 MPa which is just half of the mean tensile strength. The large fibre stress suggests that the interfacial shear stress at the fibre–matrix interface would be also large. Hence, it is reasonable to infer that sliding mode debonding may occur at the fibre/matrix interfaces. In fact, interfacial failure problem has been a central issue in the field of composite mechanics.

However, the interfacial failure was not considered in this study, because the interfacial shear stress could not be determined in the frame of the NLMS-FEA scheme. It is practically an important question to what extent local interface debonding will affect the global failure behaviour of the laminate. If local debonding at the fibre/matrix interface once takes place, this will cause an abrupt change in the fibre stress due to the extinction of the load transfer at the interface site. However, this situation will not lead to uncontrolled fibre fracture since the fibres are stressed under strong compression. Fibre fracture is hardly expected for the current micro-scale stress state. The interfacial debonding will merely redistribute the local stresses without causing any progressive failure development which might give impact on the global strength.

In the practice of FMMC fabrication, the fibre–matrix interface is optimised by means of a thin titanium film. This film forms a stable carbide reaction layer which furnishes with strong bonding strength and high frictional resistance. Furthermore, compressive normal stress is acting on the fibre–matrix interface due to the strong thermal contraction of the copper matrix upon cooling [30]. In this case, the frictional stress is still increased. Therefore, interfacial debonding and the fibre push-out phenomenon will not be the prevailing failure modes since the stored strain energy will be preferentially dissipated via plastic flow in the ductile matrix.

At 700 °C, the flow stress of the CuCrZr alloy falls to about 100 MPa. The computed matrix von Mises stress suggests that considerable plastic flow took place in the matrix. The consequence of the plastic deformation of the matrix is shown in the next figure.

The evolution of the internal variables and the damage indicator at the circle position is plotted in Fig. 11. The internal variables are the thermodynamic state parameters which determine the free energy of the material. The so-called damage indicator stands for a measure of the ductile damage density. The ductile damage in a soft metal is initiated by formation and coalescence of micro-voids. It is usually characterised by two major factors: accumulation of the plastic strains and the hydrostatic stress state. The mathematical expression of the damage indicator is found in the literature [31]. The damage indicator was scaled with an empirical coef-

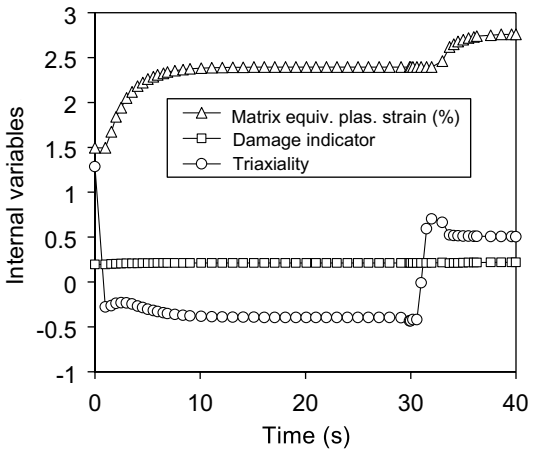

Fig. 11. Evolution of the ductile damage indicator, the stress tri-axiality and the equivalent plastic strain in the matrix during the thermal load cycle (circle position in Fig. 3).

ficient from zero to unity which corresponds to a void-free virgin state and the onset of micro-crack formation, respectively. The latter point was then identified to be the failure begin. The stress tri-axiality parameter denotes the hydrostatic stress normalised by the equivalent stress.

The ductile damage indicator for the matrix remained nearly constant and did not exceed 0.2. The ductile damage was mostly developed by the residual stress. Actually, the heat flux load did not cause any further damage, although the equivalent plastic strain was substantially accumulated during the thermal load cycle. This behaviour was attributed to the compressive hydrostatic stress state prevailing in the matrix during the heat flux loading. In the compressive hydrostatic state the growth and coalescence of micro-voids are suppressed.

Together with the compressive fibre stress, the compressive hydrostatic stress in the matrix is an advantageous feature of the current design concept.

It should be noted that the global apparent permanent deformation of the FMMC was very small. This is due to the extremely strong apparent strain hardening of the FMMC. Such a characteristic hardening behaviour is in fact common to all FMMCs regardless of their matrix yield stress. The high strain hardening rate originates from the large elastic strain energy of the high modulus fibres and the load transfer at the fibre–matrix interface [18]. It was predicted that the global apparent flow stress of the FMMC would reach nearly 500 MPa even at 700 °C already for the global strain of 0.5% [22].

The results presented above were obtained for the single heat load cycle. In order to simulate many load cycles, the plasticity model used for the micro-mechanics algorithm should be extended to consider the non-linear kinematic hardening effect. This will be the future perspective of this study.

4.6. Fracture mechanical features

The singular stress fields at the free surface edge of the interface promote the crack initiation [32]. When a crack has been formed, the stress intensity at the crack tip is decisive for the integrity of the whole joint system. Hence, the assessment of the structural integrity is closely related to the interfacial fracture problem. In this context, the fracture mechanical effect of the FMMC layer is an important concern.

To this end, the fracture mechanical parameters for the interface of the two systems were computed and compared. All fracture mechanical parameters presented here were obtained based on the elastic assumption.

At first, the stress singularity in the vicinity of the free surface edge of the perfectly bonded interface is discussed. The intensity of the singular stress field is a measure of the driving force for the crack initiation. The singular stress fields can be expressed by Blancard and Ghoniem [33]

$$\sigma_{ij}(r) \propto K \cdot r^{-\omega}. \tag{2}$$

In this formulation, σ_{ij} are the stress components along the interface, r the distance from the free surface, K the stress intensity factor and ω denotes the singularity exponent. The quantity σ_{ij} is a strong decay function of r and K and ω characterise the shape and the strength of the singular fields. They are determined by material properties, geometry and applied loads.

In the case of the W/FMMC/CuCrZr system, K and ω were identified to be -6.07 (MPa/°C) and 0.0586, respectively, whereas they were -4.25 (MPa/°C) and 0.099 for the W/CuCrZr system. The trend of the two parameters looks reciprocal. In this case, priority should be put on ω, for it affects the singularity more strongly than K. The FMMC interlayer decreased the value of ω by 41%.

Next, the fracture-mechanical effect of the FMMC layer on an interfacial crack was investigated. Using the commercial FEA code ABAQUS, the strain energy release rate of an edge interface crack was computed for the two systems. For brevity, a homogenised elastic composite layer was assumed. The details of the computational technique are found in the literature [34]. The J integral values of the edge interface crack (at the triangle position in Fig. 3) for the two systems are compared in Fig. 12, for duration of the heat load cycle. The result shows that the FMMC layer reduced the magnitude of the J integral by 35%. Relaxation of the crack loading was notable only in the cooling phase. This is because the crack tip deformation was effectively suppressed during the heating phase due to the complete crack face

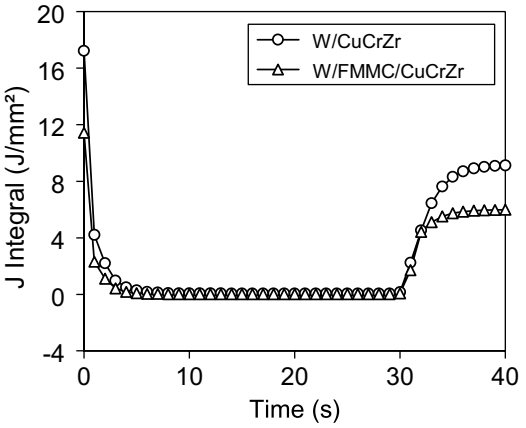

Fig. 12. J integral values of the edge interface cracks in the W/FMMC/CuCrZr system and in the W/CuCrZr system (triangle position in Fig. 3).

closure. The edge crack underwent in the cooling phase both opening and sliding fracture modes in the same ratio.

Estimations of the singularity exponent ω and the J integral demonstrate that the FMMC layer reduced the driving force for the crack initiation and propagation at the bond interface.

5. Summary and conclusions

Enhancement of divertor performance for future reactors necessarily demands an advanced heat sink material. In view of both high-temperature strength and thermal conductivity, the fibrous copper composites can be a promising candidate material for the divertor heat sink. In this study, a flat tile type divertor was investigated which consists of tungsten armour, an actively cooled copper heat sink and a composite interlayer inserted into the bond interface. Cross-ply laminate of the fibre-reinforced copper matrix composite was employed for the interlayer.

The design feasibility of this divertor concept was quantitatively evaluated in terms of structural effects and failure behaviour. To this end, elastic–plastic multi-scale finite element analysis was carried out where the thermal stresses and the damage could be traced on micro- as well as macroscopic scales. Fracture mechanical simulation was also carried out. Heat flux load of $15\,MW/m^2$ and coolant temperature of 250 °C were assumed. The stress-free temperature was assumed to be 700 °C. For comparative examination a reference divertor system without composite layer was also analysed. Comparative thermal analyses showed that the temperature difference between the two systems was small. This indicated that the influence of the composite layer on the heat removal capability of the component was insignificant for the considered heat flux load.

The tungsten armour stress in the interface region was notably increased by the stiff composite layer during the thermal loading. This negative effect was ascribed to the forced bending due to the steep temperature gradient. On the contrary, the influence of the composite layer on the heat sink stress was fairly weak.

Within the frame of the multi-scale analysis, the laminate stress could be spatially resolved into the lamina stresses for individual lamina stacking positions. The meso-scale stress profile in the composite laminate was obtained with a resolution of the lamina thickness. This profile revealed that significant stress gradient was existing even in the single laminate element.

The stresses for the fibres and the matrix were identified by means of the micro-scale stress analysis. The fibre stress was compressive and far smaller than its mean tensile strength. The damage indicator for the matrix reached only 20% of the critical value required for crack initiation. This benign damage behaviour was attributed to the compressive hydrostatic stress state in the matrix which would suppress the growth and coalescence of micro-voids. This result indicates that the reactor-relevant heat flux load would not induce any progressive fibre fracture or serious matrix damage in the copper composite laminate while the stress concentration domain near the bond interface could be effectively strengthened.

The fracture mechanical analysis demonstrated that the composite layer reduced the driving force for initiation and propagation of an interfacial crack to a considerable extent.

It can be concluded that the current divertor concept with composite reinforcement offers favourable structural features which contribute to an enhancement of the component performance.

References

[1] G. Kalinin, V. Barabash, A. Cardella, J. Dietz, K. Ioki, R. Matera, R.T. Santoro, R. Tivey, J. Nucl. Mater. 283–287 (2000) 10.
[2] ITER team, ITER-FEAT Final Design Report (2001).
[3] G. Federici, J.P. Coad, A.A. Haasz, G. Janeschitz, N. Noda, V. Philipps, J. Roth, C.H. Skinner, R. Tivey, C.H. Wu, J. Nucl. Mater. 283–287 (2000) 110.
[4] E.E. Bloom, J. Nucl. Mater. 258–263 (1998) 7.
[5] R.F. Mattas, D.L. Smith, C.H. Wu, T. Kuroda, G. Shatalov, J. Nucl. Mater. 191–194 (1992) 139.
[6] A. Li Puma, L. Giancarli, Y. Poitevin, J.-F. Salavy, P. Sardain, J. Szczepanski, Fus. Eng. Des. 61&62 (2002) 177.
[7] V. Barabash, G. Federici, M. Rödig, L.L. Snead, C.H. Wu, J. Nucl. Mater. 283–287 (2000) 138.
[8] B.N. Singh, J. Nucl. Mater. 258–263 (1998) 18.

[9] I. Smid, M. Akiba, G. Vieider, L. Plöchl, J. Nucl. Mater. 258–263 (1998) 160.
[10] H. Bolt, V. Barabash, G. Federici, J. Linke, A. Loarte, J. Roth, K. Sato, J. Nucl. Mater. 307–311 (2002) 43.
[11] K. Krieger, X. Gong, M. Balden, D. Hildebrandt, H. Maier, V. Rohde, J. Roth, W. Schneider, J. Nucl. Mater. 307–311 (2002) 139.
[12] M. Rödig, W. Kuehnlein, J. Linke, M. Merola, E. Rigal, B. Schedler, E. Visca, Fus. Eng. Des. 61&62 (2002) 135.
[13] J.J. Cordier, Fus. Eng. Des. 61&62 (2002) 71.
[14] K. Masaki, M. Tanikuchi, Y. Miyo, S. Sakurai, K. Sato, K. Ezato, H. Tamai, A. Sakasai, M. Matsukawa, S. Ishida, N. Miya, Fus. Eng. Des. 61&62 (2002) 171.
[15] H. Renner, J. Boscary, V. Erckmann, H. Greuner, H. Grote, J. Sapper, E. Speth, F. Wesner, M. Wanner, Nucl. Fus. 40 (2000) 1083.
[16] G.M. Kalinin, S.A. Fabritsiev, B.N. Singh, S. Tahtinen, S.J. Zinkle, J. Nucl. Mater. 307–311 (2002) 668.
[17] D.L. Smith, M.C. Billone, S. Majumdar, R.F. Mattas, D.K. Sze, J. Nucl. Mater. 258–263 (1998) 65.
[18] T.W. Clyne, P.J. Withers, in: An Introduction to Metal Matrix Composites, Cambridge University, Cambridge, 1993, p. 71.
[19] C. Leyens, M. Peters, W.A. Kaysser, Adv. Eng. Mater. 2 (2000) 265.
[20] J.H. You, H. Bolt, J. Nucl. Mater. 305 (2002) 14.
[21] J.H. You, H. Bolt, J. Nucl. Mater. 307–311 (2002) 74.
[22] J.H. You, O. Poznansky, H. Bolt, Mater. Sci. Eng. 344 (2003) 201.
[23] K. Tanaka, T. Mori, Acta Metall. 23 (1973) 571.
[24] A.C. Gavazzi, D.C. Lagoudas, Comput. Mech. 7 (1990) 13.
[25] ABAQUS 6.4, Analysis User's Manual, ABAQUS (2003).
[26] H.E. Pettermann, A.F. Plankensteiner, H.J. Böhm, F.G. Rammerstorfer, Comput. Struct. 71 (1999) 197.
[27] R.W. Neu, Int. J. Plast. 12 (1996) 361.
[28] J.H. You, H. Bolt, J. Nucl. Mater. 299 (2001) 9.
[29] J. Mencik, Silikaty 32 (1988) 1.
[30] J.H. You, O. Poznansky, J. Mater. Sci. 39 (2004) 2121.
[31] S.R. Gunawardena, S. Jansson, F.A. Leckie, ASME AD 22/AMD 122 (1991) 23.
[32] J.H. You, H. Bolt, J. Nucl. Mater. 299 (2001) 1.
[33] J.P. Blancard, N.M. Ghoniem, J. Nucl. Mater. 172 (1990) 54.
[34] J.H. You, H. Bolt, Fus. Eng. Des. 65 (2003) 483.
[35] ITER Material Properties Handbook, ITER Document No. S74RE1 (1997).